Land use and land cover classification for Dang district Nepal using satellite imagery and machine learning on google earth engine

Abstract

Land use land cover classification (LULC) is a key tool for accessing, monitoring and management of natural resources. Advanced remote sensing technologies such as satellite imageries and machine learning algorithms have been widely used for LULC classification around the globe. This study was aimed to compare and analyze the performance of Random Forest (RF) and Classification and Regression Tree (CART) algorithms for LULC classification of Dang district using Landsat-9 and Sentinel-2 imageries of the year 2023 on Google Earth Engine (GEE) platform. During the study, satellite images were accessed and filtered by predetermined region of interest, date, cloud percentage (<10%) and spatial resolution (30m) followed by cloud masking and median composite. Several satellite indices including normalized difference vegetation index (NDVI), normalized difference built up index (NDBI), modified normalized difference water index (MNDWI) and barren soil index (BSI) were computed and used to detect five different LULC classes i.e., crop lands, water bodies, forest and shrubs, settlements, and barren and sandy lands. The CART model classified the Landsat-9 and Sentinel-2 imageries more accurately with overall accuracies of 97.43% and 96.41% as compared to RF model i.e., 95.71% and 95.71 respectively. Similarly, the Kappa coefficient for CART was 0.97 for Landsat-9 and 0.95 for Sentinel-2 imageries while that of RF was 0.94 for both image sources. The results indicate that CART performed comparatively better than RF under same level of resolution. The current study suggests government stakeholders and policymakers to employ LULC as major key tool for sustainable land management, ecological conservation, and socio-economic development and addressing global concerns such as urbanization and climate change.

Keywords: LULC, Machine Learning, GEE, Random Forest, Classification and Regression Tree

Introduction

Land use and land cover are different but interchangeable terms. Land cover refers to the natural state of physical earth surface such as vegetation, wetlands, soil and settlements while land use indicates the purposive utilization pattern of land resource by human beings (Zhang and Li, 2022). Land use land cover (LULC) classification is the rigorous process of grouping the earth surface based on its use pattern and covering. LULC mapping is crucial for land use planning and management, environmental assessment, vulnerability and climate change (Talukdar et al., 2020a and Tung et al., 2023). It also helps to determine the way of land use transformation over the time period. Rapid changes in LULC are prominent in developing regions (Tariq et al., 2023) due to increasing population, urbanization and human interventions on natural resources, due to which frequent surveying of earth surface is important. Traditional methods such as visual observation and field surveying are capable of classifying land use and cover pattern accurately but are considered to be expensive and inefficient (Ilbrahim, 2023). To overcome this problem, modern technological advancements such as remote sensing are essential. Remote sensing is the technique of gathering information about earth surface without physical contact. Satellites, uncrewed air vehicles, passive and active sensors are used to collect the required information which ultimately processed and analyzed to derive useful insights.

Google earth engine is an open-source web-based cloud computing system that provides global time series multi-satellite geo-data for geo-spatial applications (Kumar and Mutanga, 2018 and Gorelick, 2017). It is known for its rapid computing abilities, accessible large storage system and web-based portal which allows clients to process petabyte data through normal devices (Kumar and Mutanga, 2018). GEE consists a large repository of satellite remote sensing data such as Moderate resolution imaging spectroradiometer (MODIS), Sentinel, Landsat, Cropland, Land cover which are widely applied in several concerned fields including agriculture, hydrological management, land use land cover, climate change, disaster management, urbanization and ecological sciences (Xiong et al., 2017; Huang et al., 2017; Devries et al., 2020; Ivushkin et al., 2019, Ahemad et al., 2023 and Bullock et al., 2020). Although the quality of earth observatory data ranges from low to very high depending upon the remote sensing technologies, high resolution imageries are rarely available due their affordability (Stoian et al., 2019) but, medium resolution data from satellites such as Landsat-8,9 and Sentinel-1,2 can be employed for LULC classification purposes (Zhao et al., 2024). Machine learning comes at the intersection of computer science and data science (Jordan and Mitchell, 2015). It exhibits the ability of performing assigned task without external programming (Mahesh, 2019). Random Forest (RF) and Classification and Regression Tree (CART) are supervised machine learning models which are capable of making decisions based on training datasets. These models are capable classifying land use and land cover pattern using satellite imageries including Sentinel and Landsat images in GEE platform precisely (Oliveira et al., 2012; Choubin et el., 2019). However, their results may vary with imagery sources and their quality, number and distribution of training and testing data (Avci et al., 2023).

Previously, several geospatial researchers have conducted numerous studies using the imageries of Landsat and Sentinel satellites and machine learning algorithms such as random forest, classification regression tree and even support vector machine. For instances, Zhao et al., 2024 comparatively analyzed the performance of three different machine learning models including RF and CART for Sentinel-2 imagery. Similarly, Avci et al., 2023 also performed similar study with

RF and SVM for Sentinel-2 imageries. Both of the studies shown the performance abilities of different machine learning models using same geospatial data, which might result differently when employed for different data sources. Furthermore, Lokika et al., 2021 also studied the performance of machine learning models for Landsat-8 and Sentinel-2 imageries at 30 and 10 meters of resolutions and resulted RF as superior classifier for both of the image sources. However, resulted outcome might be due to variation of image resolution between image sources (Zheng et al., 2021). Since the district consists of fertile soil for agriculture, dense forest and shrub lands and water resources in its plain lands, valley and hilly terrains it becomes highly prone urbanization, deforestation and other human induced land use and land cover changes over time. Unfortunately, LULC classification of Dang district are rarely available in documented formats suggesting huge research gap. Poudel and Rawat, 2023 conducted a study in Ghorahi sub-metropolitan municipality of Dang district for urban area extension using supervised maximum-likelihood (SML) and supervised vector machine (SVM) and Landsat-8 images. The machine learning models used in the particular study are considered to be comparatively less reliable than RF (Zhao et al., 2024) which have generated more accurate results in several studies. Therefore, to overcome the huge research and methodological gap for LULC classification in the region of interest and to evaluate the performance ability of RF and CART model, for Landsat-9 and Sentinel-2 imageries at equal resolutions of 30 meters, this study was performed.

Study Area

In this study, land use land cover classification and performance analysis of Dang district (Latitude: 27.633^0N to 28.383^0N and Longitude: 82.217^0E to 83.250^0E) of Lumbini province Nepal was performed. Dang district is located in mid hills of Nepal surrounded by Siwalik ranges in the north and flat plane lands in the south with elevation ranging from 213 meters to 1500 meters above the sea level. It shares the tropical to subtropical climate with hot summer monsoon and mild winter. The district is rich in forest and water resources, biodiversity, and fertile plain lands for agriculture.

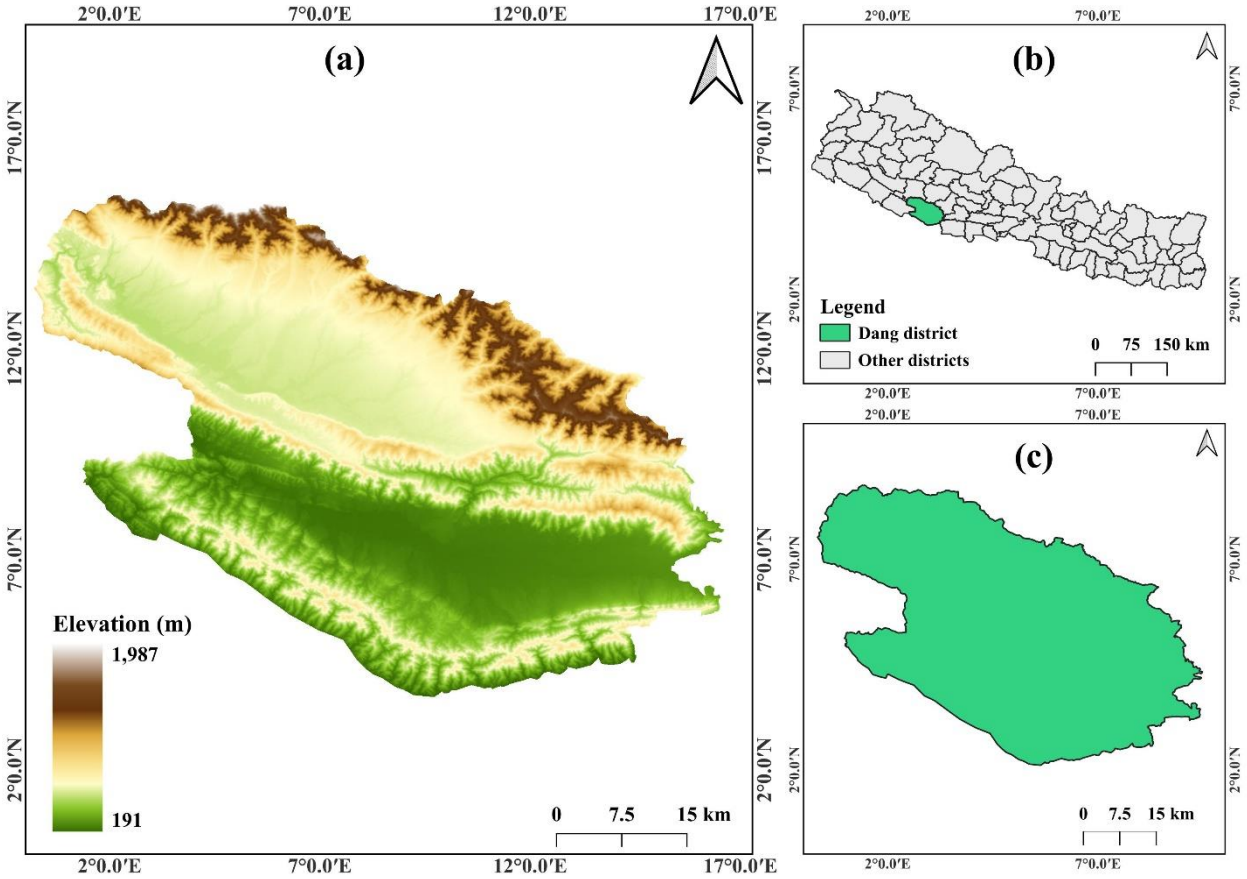

Figure 1 a. Study area with elevation estimated from Shuttle Radar Topography Mission (SRTM) data. **b.** District boundaries Dang district. **c.** Dang district used as region of interest (ROI).

Materials and methods

Datasets

The multispectral imageries of Landsat-9 and Sentinel-2 satellites were accessed and purposively used for land use land cover classification in the google earth engine platform. The acquired imageries were filtered by date i.e., January to December 2023 maintaining the cloud masking of less than 10%. Landsat-9 is satellite operation managed in collaboration of NASA and USGS. It provides high resolution images crucial for monitoring and managing of land resources, water use, urban expansion, coral reef degradation and so forth. Sentinel-2 is another satellite operation owned by European space agency with up to10 meters of resolution and 13 different spectral bands.

Methodology

Each methodological procedures involved during the study were performed on Google earth engine and QGIS. The detailed methodological process of the study is depicted in **Figure 2.**

Image acquisition and filtration

In the Google earth engine platform, freely available satellite imageries from both sources i.e., Landsat-9 and Sentinel-2 were acquired. Since the repository provides bulk geospatial data, proper filtration is utmost important to maintain the quality and useability. Imported imageries of both sources were filtered separately by using date (01/01/2023 to 12/31/2023), region of interest and cloud percentage i.e., < 10%.

Cloud masking

The cloud containing pixels on satellite imageries are crucial elements to be considered during earth observatory, atmospheric and environmental studies. During atmospheric and meteorological studies, cloud contaminated pixels provide useful information, however should be removed or masked during land surface monitoring (Anzalone et al., 2024) to maintain the quality of imageries. In this study, "CFMASK" and "maskLowQA" functions inbuilt in GEE were employed for cloud masking in Landsat-9 and Sentinel-2 images respectively.

Computation of spectral indices

Several spectral indices were computed in GEE using available bands as described below.

Normalized difference vegetation index (NDVI)

The Normalized Difference Vegetation Index (NDVI) is a key tool for evaluating vegetation health and land use changes using satellite images, which helps with sustainable planning. A healthier crop canopy will absorb more red light and reflect more near-infrared light, resulting in a higher NDVI value (Milella & Reina, 2024).

Formula: NDVI is calculated as;

$$NDVI = \frac{NIR - RED}{NIR + RED} \quad \text{Equation 1.}$$

Where, RED refers to the reflectance in the visible red spectrum, while NIR denotes the reflectance in the near-infrared spectrum. The near-infrared band covers wavelengths from 750 to 1300 nm, the red band ranges from 600 to 700 nm (Huete et al., 1994). NDVI values range from -1 to +1, with higher values indicating denser and healthier vegetation, while lower values indicate sparse or stressed vegetation (Milella & Reina, 2024).

Normalized difference built-up index (NDBI)

NDBI is a crucial tool for distinguishing built-up areas from vegetation and other land cover types, using satellite images, providing insights into urban growth and patterns (Yasin et al. 2022). NDBI is determined using the SWIR1 and NIR bands of the Landsat sensor (Guha et al., 2021)

Formula: NDBI is calculated by;

$$NDBI = \frac{(SWIR - NIR)}{(SWIR + NIR)} \quad \text{Equation 2.}$$

Where, the Normalize Difference Build-up Index value lies between -1 to +1. A negative NDBI value indicates the presence of water bodies, while higher values signify built-up areas. Vegetation is associated with lower NDBI values. NDBI values between 0.1 and 0.3 indicate built-up areas, while values greater than 0.25 suggest bare lands (Zha et al., 2003).

Modified normalized difference water index (MNDWI)

Modified Normalized Difference Water Index (MNDWI) is a remote sensing tool that enhances the delineation of water bodies in satellite imagery by effectively distinguishing between water, vegetation, and urban areas. MNDWI is determined using the GREEN and MIR bands instead of a NIR band.

Formula: MNDWI is calculated by;

$$\text{MNDWI} = \frac{(Green - MIR)}{(Green + MIR)} \qquad \text{Equation 3.}$$

Where, it reveals that the average digital number of TM band 5, representing middle infrared (MIR) radiation and Modified Normalize Difference Water Index (NDWI) value lies between -1 to 1. Water exhibits higher positive values in the MNDWI because it absorbs more mid-infrared (MIR) light compared to near-infrared (NIR) light. Built-up areas display negative values. According to Jensen 2004, Soil and vegetation show negative values because soil reflects more mid-infrared (MIR) light than near-infrared (NIR) light.

Enhanced vegetation index (EVI)

The enhanced vegetative index (EVI) is a satellite-derived index used to measure vegetation health, density, and productivity. It is designed to optimize the vegetation signals and improve the sensitivity to high biomass regions, while minimizing background signals and atmospheric effects, compared to the widely used NDVI and comparatively less sensitive to different soil background (Huete et al., 2002).

Formula: It is calculated by;

$$\text{EVI} = 2.5 * \frac{NIR - Red}{(NIR + 6 * Red - 7.5 * Blue) + 1} \qquad \text{Equation 4.}$$

Bare soil index (BSI)

The Bare Soil Index (BSI) is a tool used in the remote sensing to identify and quantify bare soil area in satellite imagery. It accurately classifies and differentiate bare soil and other land covers, like vegetation, water bodies and built-up areas (Nguyen et al., 2021 & Somanathan et al., 2024).

Formula: It is calculated by;

$$\text{BSI} = \frac{(\text{SWIR} + \text{Red}) - (\text{NIR} + \text{Blue})}{(\text{SWIR} + \text{Red}) + (\text{NIR} + \text{Blue})} \qquad \text{Equation 5.}$$

Where, SWIR= short-waved infrared band and NIR= near- infrared band. Its values range between −1 and 1, where, higher value indicates a higher change on bare soil and lower value indicates a higher vegetation.

Median composite

Compositing is the process of creating a single representative image from multiple layers of images of a particular region of interest using specific mathematical procedure which helps to reduce the spatial noise (Roberts et al., 2017). Several statistical tools such as mean, median, mode, minimum and maximum are available for compositing purpose, however, median is considered to be more efficient in case of noisy geospatial data.

Creating training points

Training datasets were created in the composite images of both Landsat-9 and Sentinel-2 using polygon tool in GEE. For this purpose, separate layer for each LULC classes were created and each area was marked accurately, which were further used to train the machine learning models. The numbers of polygons for crop lands, water bodies, forest and shrub lands, built up and barren lands were 143, 130, 100, 175 and 60 respectively. The procedure was adopted as suggested by Avci et al., 2023.

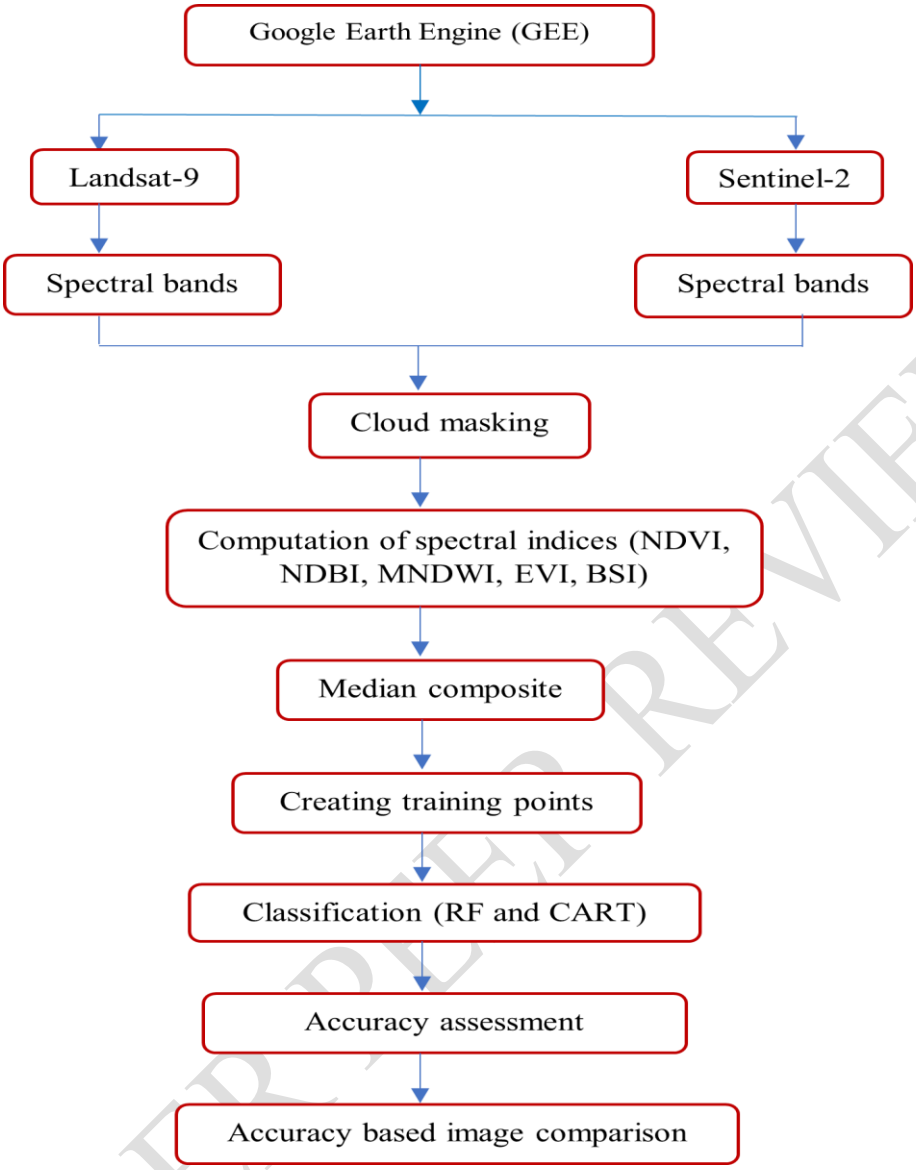

Figure 2. Methodology of Land Use Land Cover (LULC) classification on Google Earth Engine (GEE) platform.

Machine learning algorithms

Machine learning models allow us to integrate geospatial datasets with machine learning algorithms for LULC classification (Zhao et al., 2024) and developing decision support system. However, their performance accuracy is crucially important. Although several machine learning models are available for classification of imageries based on available spectral bands, RF and CART models were employed in this study.

Random Forest (RF) Classifier

Random forest is extensively employed in classification and regression tasks due to its wide application features with high classification accuracies. RF is capable of dealing with high-

dimensional datasets, complex decision boundaries and mitigating over-lifting issues (Sultana and Inayathulla, 2022). The operating mechanisms of RF resembles with trees inside the forest. Each tree as a part of whole model, makes classification decision based on the training datasets which finally becomes the prediction of overall classifier (Donges, 2024).

Classification and Regression Tree (CART) Classifier

CART developed by (Breimen et al., 1984) is a simple binary decision-making tool based on if-then scenarios based on hierarchical decision trees (Shetty, 2019). Such type of models splits the training data into two groups or subsets resembling with nodes of the trees which leads to separate branching and is continued until the terminal node is formed (Loukika et al., 2021). In this model, a single decision tree is formed and outputs depends on sample size each classification classes. Moreover, high dimensionality of datasets may lead to complex tree architecture thereby reduced accuracy.

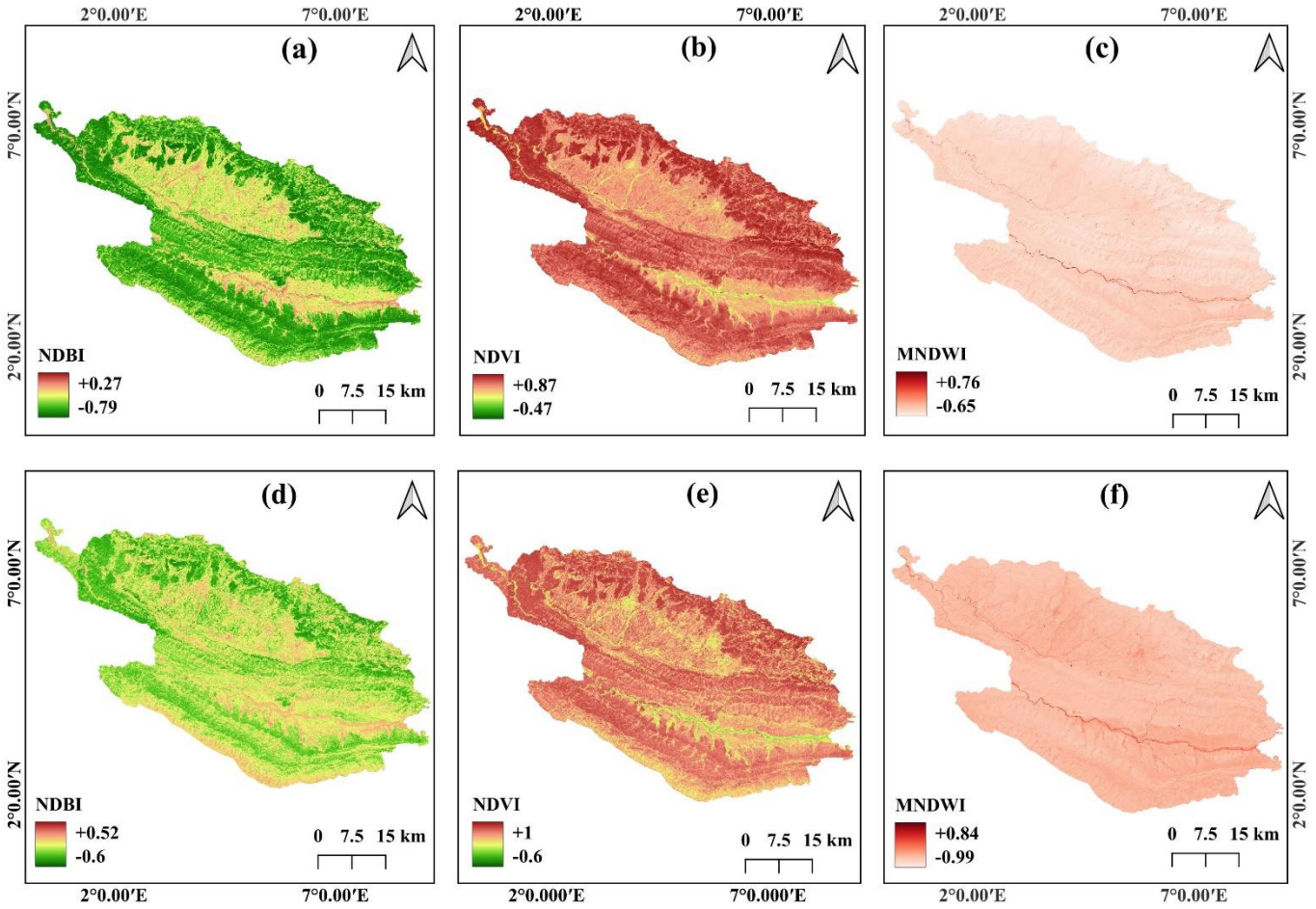

Figure 3. Depiction of major satellite indices. **a.** Normalized Difference Built Index (NDBI) **b.** Normalized Difference Vegetation Index (NDVI) and **c.** Modified Normalized Difference Water Index (MNDWI) using Landsat-9 imageries. **d.** Normalized Difference Built Index (NDBI) **e.** Normalized Difference Vegetation Index (NDVI) and **f.** Modified Normalized Difference Water Index (MNDWI) using Sentinel-2 imageries.

Accuracy assessment

The performance of each machine learning models was evaluated with accuracy assessment after classification of composite image. For this purpose, imageries were divided into training (80%) and testing (20%) datasets using point geometry in google earth engine. Confusion matrix was employed for validation and rating of image categorization as suggested by Zhao et al., 2024. Following mathematical equations were used for calculation of Kappa coefficient, Producer accuracy, User accuracy and Overall accuracy.

$$OA = \left(\frac{Pc}{Pn}\right) \times 100 \qquad \text{Equation 6.}$$

Where, Pc is the correctly classified pixel numbers and Pn is the total pixel numbers.

$$k = \frac{N \sum_{i=1}^{r} x_{ii} - \sum_{i=1}^{r} (x_{i+} \times x_{+i})}{N2 \sum_{i=1}^{r} (x_{i+} \times x_{+i})} \qquad \text{Equation 7.}$$

Where, N= total number of observations, r = number of rows and columns in error matrix, x_{ii} = number of observations in row *i* and column *i*, x_{i+} = marginal total of row *i*, x_{+i} = marginal total of column *i*. The producer accuracy was estimated by the ratio of correctly categorized pixels to total number of pixels for each class. The magnitude ranges between – 1 to + 1 where value greater than + 0.5 was acceptable as categorization (Talukdar et al., 2020a).

Results

LULC classification by Random Forest and Classification Regression Tree

Land use land cover scenario of Dang district was classified by using two different supervised machine learning models i.e., Random Forest (RF) and Classification and Regression Tree (CART) for comparative analysis of their performance. Area distribution of land use land cover categories as generated by RF and CART models for Landsat-9 and Sentinel-2 are described as below **(Figure 4,5,6 and 7)**.

Landsat-9

The classifications of Dang district using Landsat-9 imageries with RF and CART models are shown in **Figure 4 & 6**. According to the classification using RF, 159.62 km^2 was classified as forest and shrubs, 75.09 km^2 as crop lands, 52.96 km^2 as built up, 14.69 km^2 as water bodies and 3.50 km^2 as barren land. Similarly, classification results with CART model revealed that 155.74 km^2, 69.41 km^2, 61.02 km^2, 9.93 km^2 and 9.76 km^2 of land area were classified as forest and shrubs, built up, crop lands, barren lands and water bodies respectively.

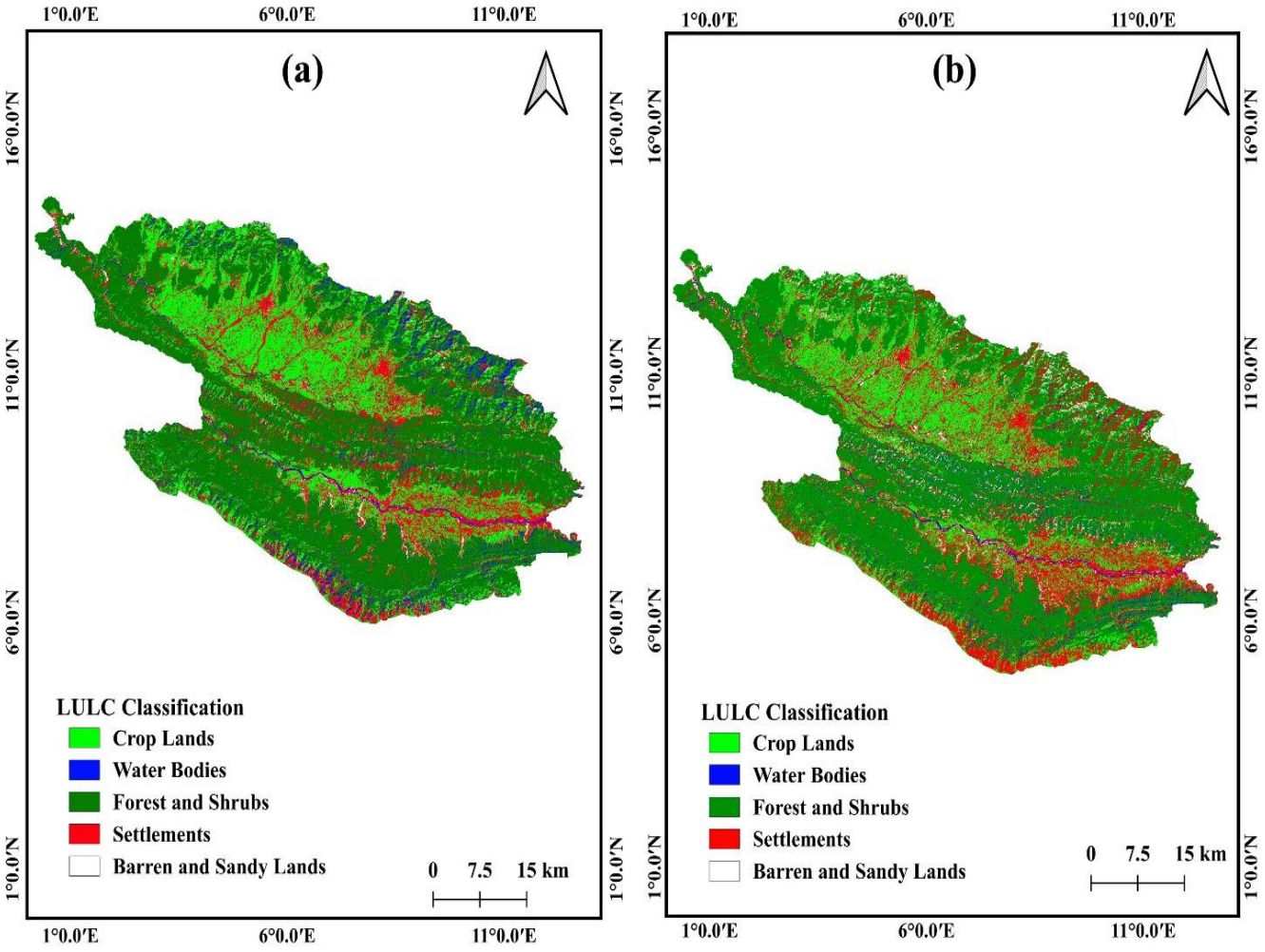

Figure 4. Land use land cover (LULC) maps of Landsat-9 imageries. **a.** using RF and **b.** CART models for the year 2023.

Sentinel-2

The generated results of LULC of Dang district with Sentinel-2 imagery, using RF and CART models are shown in **Figure 5 & 7**. In case of RF model, 154.23 km^2 of area was classified as forest and shrubs, 76.41 km^2 as crop lands, 40.35 km^2 as built up, 22.09 km^2 as water bodies and 12.79 km^2 as barren land. Similarly, in case of CART model, classification results indicate that 136.19 km^2, 68.16 km^2, 52.84 km^2, 29.76 km^2 and 18.91 km^2 of areas were classified as forest and shrubs, crop lands, built up, barren lands and water bodies respectively.

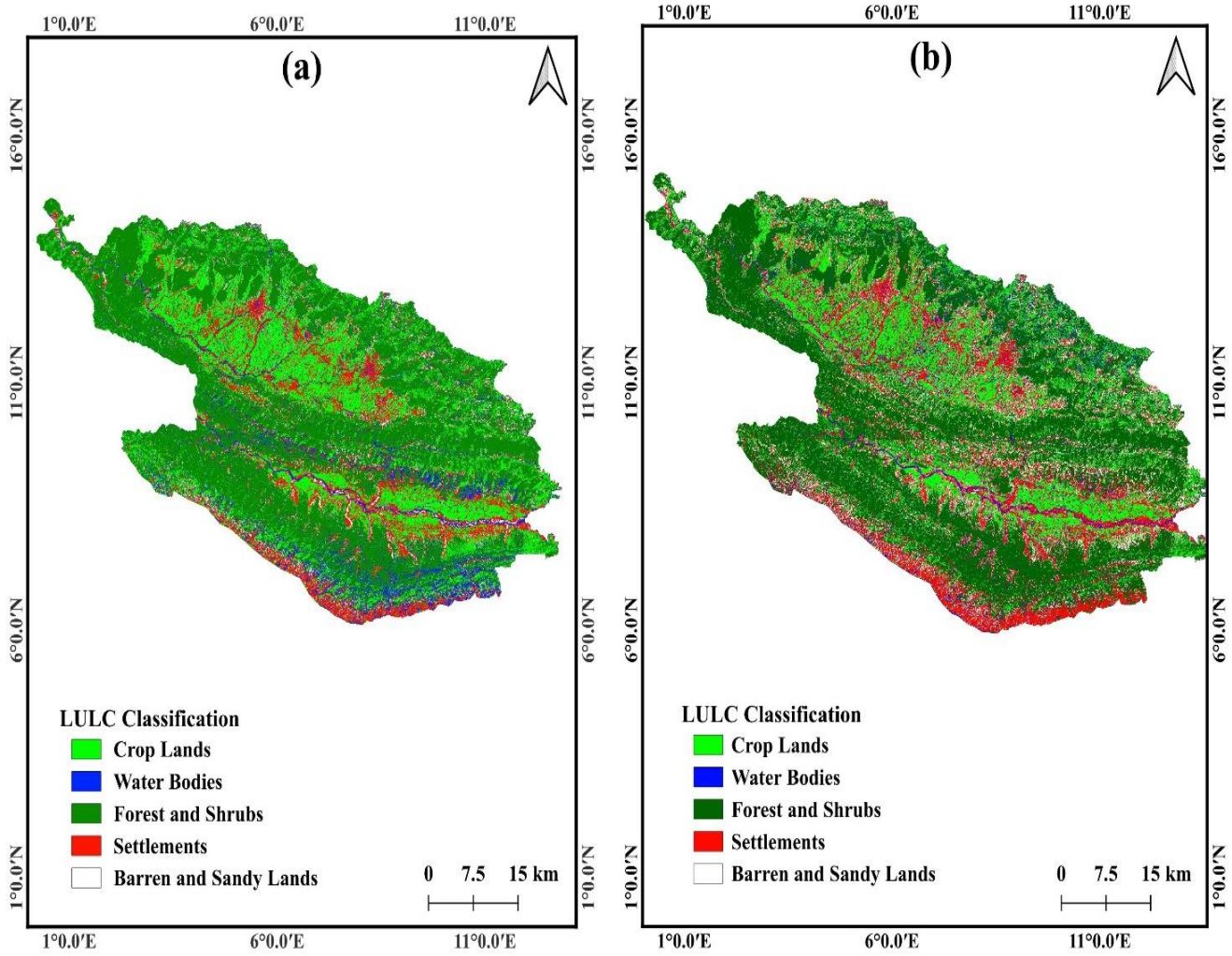

Figure 5. Land use land cover (LULC) maps of Sentinel-2 imageries. **a.** using RF and **b.** CART models for the year 2023.

Evaluation of Performance

The producer's and user's accuracy of both RF and CART model were estimated for each LULC categories. The accuracy performance of each category is described as below:

Landsat-9

Crop lands

The accuracy outcomes of crop lands using both classifiers and satellite imageries are presented in Table. Results shows that producer's accuracy and user's accuracy of crop lands generated by RF model were 98.0% and 94.0% respectively. Similarly, producer's and user's accuracy for crop lands generated by CART model were 96.0% and 100.0% respectively.

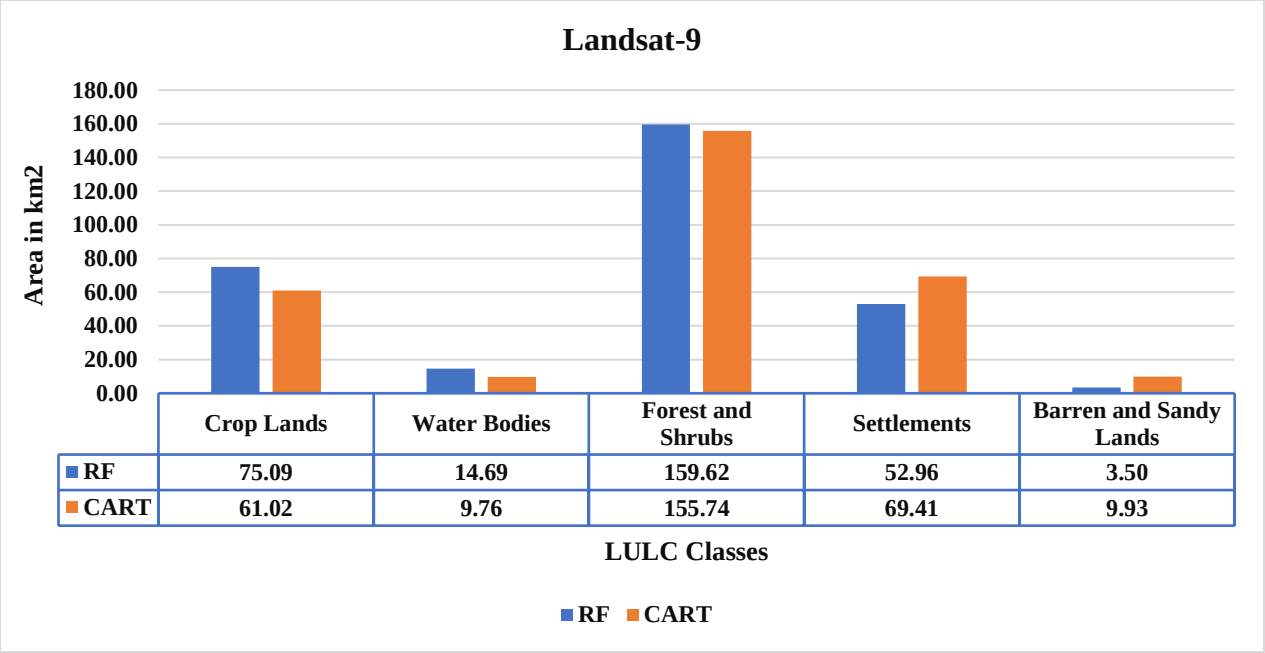

Figure 6. Area of each LULC classes estimated by RF and CART model using Landsat-9 imageries.

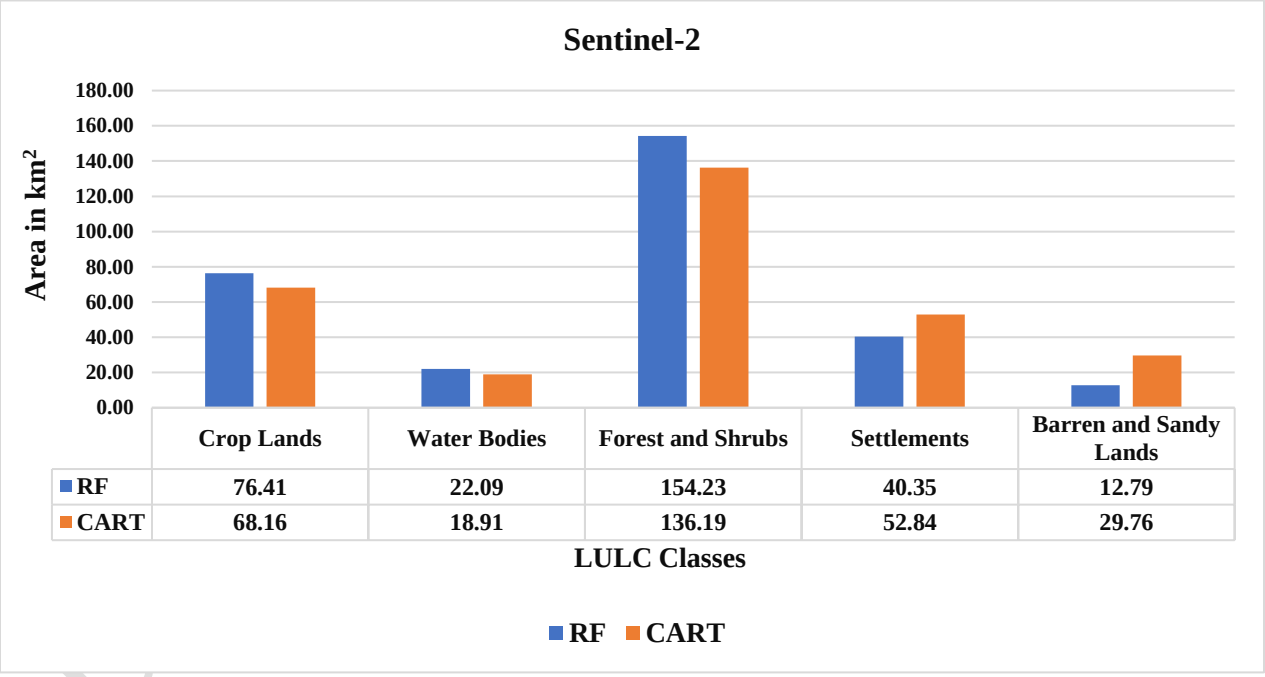

Figure 7. Area of each LULC classes estimated by RF and CART model using Sentinel-2 imageries.

Water bodies

The PA and UA for water bodies generated by RF model were 97.0% and 99.0% while for CART, 99.0% and 100.0% respectively.

Forest and shrub lands

The PA and UA for forest and shrubs extracted by RF was 99.0% and 96.0% while CART results for PA and UA for forest and shrubs were 100.0% and 98.0% respectively.

Settlements

The PA and UA for settlement areas generated by RF were 95.35% and 93.71% while CART generated 98.6% and 94.41% respectively.

Barren lands

PA and UA for barren land generated by RF were 78.0% and 100.0% whereas CART has 85.0% and 92.0% respectively. This result revealed that CART is the best machine learning technique to map barren land using landsat-9 imageries.

Sentinel-2

Crop lands

The PA and UA for crop lands generated by RF were 95.0% and 94.0% respectively. The CART result for PA and UA of crop lands were 96.0% and 98.0% indicating CART as best technique to classify the crop lands when coupled with Sentinel-2 imageries.

Water bodies

The RF classifier has extracted the 98.0% of PA and UA accuracy for water bodies using Sentinel-2 imageries whereas CART has generated PA and UA of 98.0% and 97.0% respectively. This result suggests RF as best method for classifying water bodies.

Forest and shrub lands

The PA and UA for forest and shrubs generated by RF were 99.0% and 95.0% respectively however, CART has extracted 99.0% and 100.0% of PA and UA. This also indicates CART is the best classifying method for forest and shrubs.

Settlement lands

The PA and UA for buildup lands extracted by RF are 98.0% and 94.0% respectively while CART has generated 96.0% and 93.0% of PA and UA respectively. This result suggests RF is the best method for mapping buildup lands using Sentinel-2 imageries.

Barren lands

PA and UA for barren land generated by RF are 71.0% and 93.0% whereas CART produced PA and UA of 87.0% and 92.0% using Sentinel-2 imageries. This result indicates CART is the best method for mapping barren lands using Sentinel-2 imageries.

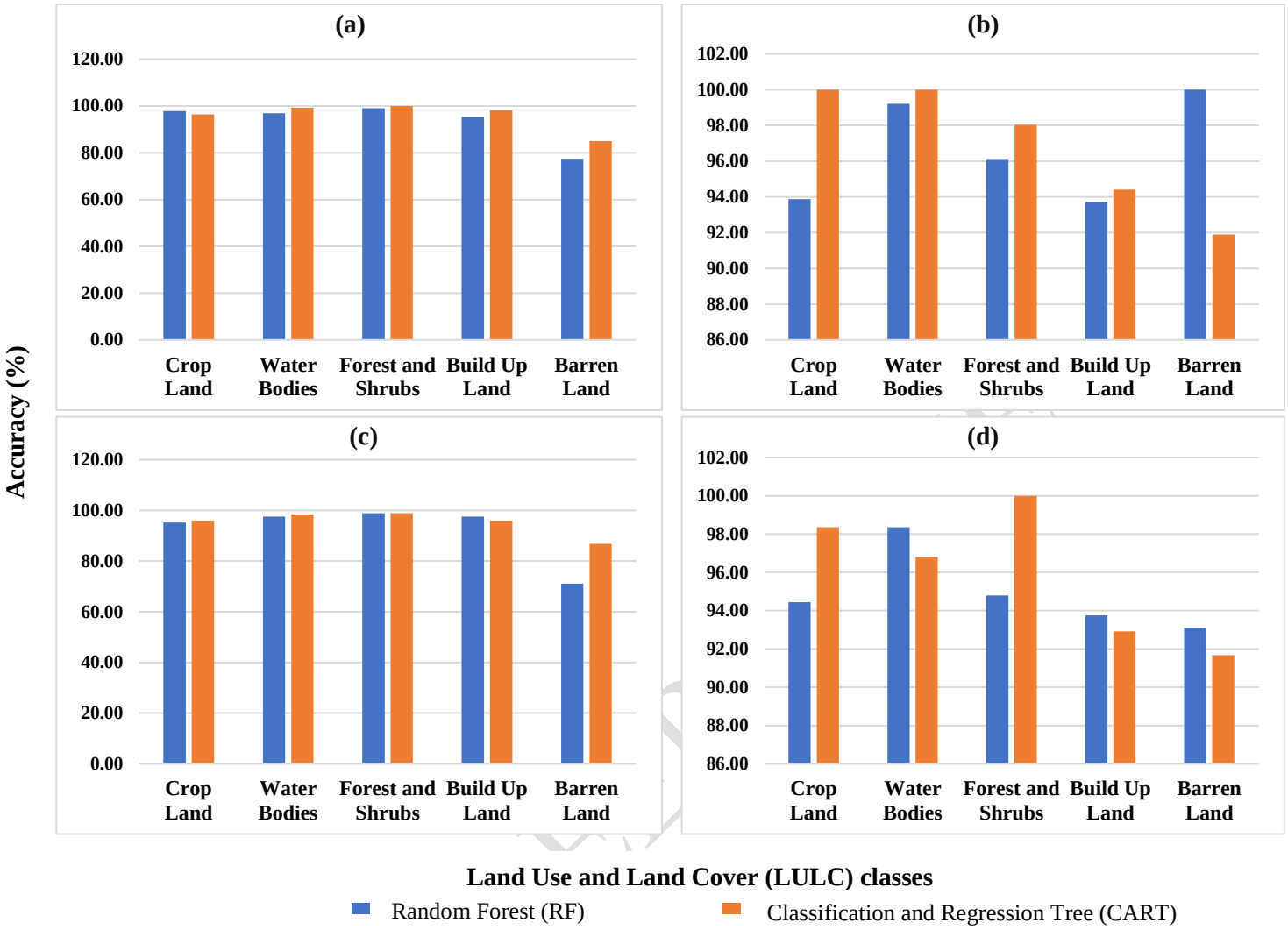

Figure 8: **a**. Producer accuracy for each LULC classes of Landsat-9 imageries using RF and CART. **b**. User accuracy for each LULC classes of Landsat-9 imageries using RF and CART. **c**. Producer accuracy for each LULC classes of Sentinel-2 imageries using RF and CART. **d**. User accuracy for each LULC classes of Sentinel- imageries using RF and CART.

Result validation

The results generated by RF and CART machine learning algorithms using Landsat-9 and Sentinel-2 imageries were validated by overall accuracy (OA) and Kappa coefficient (KC) as shown in **Table 1**. The OA and KC for RF using Landsat-9 imageries were 96.0% and 94.0% respectively. Similarly, OA and KC of RF algorithm for Sentinel-2 imageries were 95.0% and 94.0% respectively.

Furthermore, OA and Kc of CART algorithm also varied among the satellite image sources. OA and Kc of CART for Landsat-9 were 97.0% each while 96.0% and 95.0% respectively in case of Sentinel-2 imageries. The result validates that RF and CART algorithms are applicable for land use land cover mapping using both of the satellite imageries.

Table 1. Accuracy assessment of land use land cover (LULC) classes of satellite imageries using RF and CART.

Image Source	Classifier	Classes	Producer Accuracy (%)	Users Accuracy (%)	Overall Accuracy (%)	Kappa Coefficient
Landsat-9	RF	Crop Lands	97.87	93.88	95.71	0.94
		Water Bodies	96.92	99.21		
		Forest and Shrubs	99.00	96.12		
		Settlements	95.35	93.71		
		Barren and Sandy Lands	77.50	100.00		
Landsat-9	CART	Crop Lands	96.45	100.00	97.43	0.97
		Water Bodies	99.23	100.00		
		Forest and Shrubs	100.00	98.04		
		Settlements	98.26	94.41		
		Barren and Sandy Lands	85.00	91.89		
Sentinel-2	RF	Crop Lands	95.20	94.44	95.21	0.94
		Water Bodies	97.56	98.36		
		Forest and Shrubs	98.91	94.79		
		Settlements	97.56	93.75		
		Barren and Sandy Lands	71.05	93.10		
Sentinel-2	CART	Crop Lands	96.00	98.36	96.41	0.95
		Water Bodies	98.37	96.80		
		Forest and Shrubs	98.91	100.00		
		Settlements	95.93	92.91		
		Barren and Sandy Lands	86.84	91.67		

Note: RF: Random Forest, CART: Classification and Regression Tree.

Discussion

In this study, two different machine learning models i.e., RF and CART were employed to classify the land use and land cover of Dang district using Landsat-9 and Sentinel-2 data for the year 2023. From the classified images, some of the forest covered lands were classified as crop lands due to reflectance of imageries which mislead the classifier. Similar issues during land cover classification were also reported by Avci et al., 2023 and Loukika et al., 2021. Such misclassification has seen in small shrub areas at the middle of forest, which was further confirmed by site observation. Additionally, barren lands nearby rivers in the imageries were misclassified as settlements which might be due to resembling reflectance characters of sandy lands and settlement buildings. The misclassification between sandy lands and settlement areas was also confirmed by Loukika et al., 2021, which particularly happens due to seasonality of the water bodies. The coverage area of water bodies increases during monsoon and drastically reduced during winter and hot summer leaving barren sandy river banks. During generation of median

image using several multispectral imageries taken by satellites over the year, pixels of river banks resemble with that of buildings leading to minor misclassification. This reduces the accuracy of the employed machine learning models. Moreover, due to complex terrain system of the district, shadows created by high hills and dense forest in some northern and southern parts were classified as water bodies even after rigorous masking of shadow effects. This indicates that performance of machine learning models requires precise filtering of satellite imageries considering the appropriate sun angle. The performance capabilities of CART model were comparatively higher than RF either with Landsat-9 or Sentinel-2 imageries. This might be due to using both image sources at same level of resolution i.e., 30 meters. However, this result contradicts with Zhao et al., 2024, who reported the superiority of RF model over CART as they used only Sentinel-2 at the resolution of 10 meters. Similarly, Loukika et al., 2021 also have reported contradictory results where RF outperformed CART for Landsat-8 and Sentinel-2 imageries at 30 and 10 meters of resolution which might be due using different quality images. The performance accuracy classification models ultimately depend on number and preciseness of training data (Thanh & Kappas, 2018), numbers of trees and random expression (Talukdar et al., 2020a; Talukdar et al., 2020b) which might occur in our study due to same number of training samples. Moreover, RF and CART machine learning models can be used thoroughly to create the baseline for policy making for sustainable management natural resources, urban planning and mitigating the impacts of climate change.

Conclusion

Mapping of land use and land cover is utmost important for sustainable land monitoring, utilization and management. Satellite image repositories are assets collected through advanced remote sensing technologies such as satellites which help governments and related stakeholders to consider the past scenarios of earth surface before developmental project planning. Additionally, machine learning algorithms play indispensable role for LULC classification based on pixels of imageries. This study aims to estimate the performance of two different machine learning models (RF and CART) for LULC based on Landsat-9 and Sentinel-2 imageries on GEE platform. The classified images indicate that LULC classification is extremely dependent to image resolution, quality of images, classifier employed and training samples. Results shown that CART model was slightly superior in terms of image classification under both image sources (Landsat-9 and Sentinel-2) at 30 meters of resolution as compared to RF. The finding suggests image resolution, cloud masking, region of interest, selection of classifier, number of training samples should be considered for precise and reliable LULC results. Further investigations of classifiers specially under varied image resolution and appropriate shadow correction for complex terrain systems are highly suggested. In conclusion, GEE is useful tool for acquisition, processing of geospatial datasets and generating insightful outputs such as land use and land cover classification using several machine learning algorithms at national or global scale.

Disclaimer (Artificial intelligence)

Option 1:

Author(s) hereby declare that NO generative AI technologies such as Large Language Models (ChatGPT, COPILOT, etc.) and text-to-image generators have been used during the writing or editing of this manuscript.

References

1. Anzalone, A., Pagliaro, A., & Tutone, A. (2024). An Introduction to Machine and Deep Learning Methods for Cloud Masking Applications. *Applied Sciences*, *14*(7), 2887. https://doi.org/10.3390/app14072887
2. Avcı, C., Budak, M., Yağmur, N., & Balçık, F. (2023). Comparison between random forest and support vector machine algorithms for LULC classification. *International Journal of Engineering and Geosciences*, 8(1), 1-10. https://doi.org/10.26833/ijeg.987605
3. Breiman, L. (2001). Random forests. *Machine Learning*, 45, 5-32. https://doi.org/10.1023/A:1010933404324.
4. Bullock, E. L., Woodcock, C. E., & Olofsson, P. (2020). Monitoring tropical forest degradation using spectral unmixing and Landsat time series analysis. *Remote sensing of Environment*, 238, 110968. https://doi.org/10.1016/j.rse.2018.11.011
5. Choubin, B., Rahmati, O., Soleimani, F., Alilou, H., Moradi, E., & Alamdari, N. (2019). Regional groundwater potential analysis using classification and regression trees. In Spatial modeling in GIS and R for earth and environmental sciences (pp.485-498). Elsevier. https://doi.org/10.1016/B978-0-12-815226-3.00022-3
6. DeVries, B., Huang, C., Armston, J., Huang, W., Jones, J. W., & Lang, M. W. (2020). Rapid and robust monitoring of flood events using Sentinel-1 and Landsat data on the Google Earth Engine. *Remote Sensing of Environment*, 240, 111664. https://doi.org/10.1016/j.rse.2020.111664
7. Donges, N. (2024, March 8). Random forest: A complete guide for machine learning learning. Builtin. https://builtin.com/data-science/random-forest-algorithm
8. Gorelick, N., Hancher, M., Dixon, M., Ilyushchenko, S., Thau, D., & Moore, R. (2017). Google Earth Engine: Planetary-scale geospatial analysis for everyone. *Remote sensing of Environment*, *202*, 18-27. https://doi.org/10.1016/j.rse.2017.06.031
9. Guha, S., Govil, H., Gill, N., & Dey, A. (2021). A long-term seasonal analysis on the relationship between LST and NDBI using Landsat data. *Quaternary International*, *575*, 249-258.
10. Huang, H., Chen, Y., Clinton, N., Wang, J., Wang, X., Liu, C., ... & Zhu, Z. (2017). Mapping major land cover dynamics in Beijing using all Landsat images in *Google Earth Engine. Remote sensing of environment*, *202*, 166-176. https://doi.org/10.1016//j.rse.2017.02.001
11. Huete, A., Didan, K., Miura, T., Rodriguez, E. P., Gao, X., & Ferreira, L. G. (2002). Overview of the radiometric and biophysical performance of the MODIS vegetation

indices. *Remote sensing of environment*, *83*(1-2), 195-213. https://doi.org/10.1016/S0034-4257(02)00096-2

12. Huete, A., Justice, C., & Liu, H. (1994). Development of vegetation and soil indices for MODIS-EOS. *Remote Sensing of Environment*, *49*, 224 – 234.
13. Ibrahim, S. A. (2023). Improving land use/cover classification accuracy from random forest feature importance selection based on synergistic use of sentinel data and digital elevation model in agriculturally dominated landscape. *Agriculture*, *13*(1), 98. https://doi.org/10.3390/agriculture13010098
14. Ivushkin, K., Bartholomeus, H., Bregt, A. K., Pulatov, A., Kempen, B., & De Sousa, L. (2019). Global mapping of soil salinity change. *Remote sensing of environment*, *231*, 111260. https://doi.org/10.1016/j.rse.2019.111260
15. Jensen, J. R. (1996). Introductory digital image processing: a remote sensing perspective. CabiDatabase.
16. Jordan, M. I., & Mitchell, T. M. (2015). Machine learning: Trends, perspectives, and prospects. Science, 349(6245), 255-260. https://doi.org/10.1126/science.aaa8415
17. Kumar, L., & Mutanga, O. (2018). Google Earth Engine applications since inception: Usage, trends, and potential, *Remote Sensing.*, *10*, 1509. https://doi.org/10.3390/rs10101509
18. Loukika, K. N., Keesara, V. R., & Sridhar, V. (2021). Analysis of land use and land cover using machine learning algorithms on google earth engine for Munneru River Basin, India. *Sustainability*, *13*(24), 13758. https://doi.org/10.3390/su132413758
19. M, A., Ahmed, S.A. & N, H. Land use and land cover classification using machine learning algorithms in google earth engine. *Earth Sci Inform* **16**, 3057–3073 (2023). https://doi.org/10.1007/s12145-023-01073-w
20. Mahesh, B. (2020). Machine learning algorithms-a review. *International Journal of Science and Research (IJSR)*, *9*(1), 381-386.
21. Milella, A., & Reina, G. (2024). Consumer-grade imaging system for NDVI measurement at plant scale by a farmer robot. *Measurement*, *234*, 114817.
22. Nguyen, C. T., Chidthaisong, A., Kieu Diem, P., & Huo, L. Z. (2021). A modified bare soil index to identify bare land features during agricultural fallow-period in southeast Asia using Landsat 8. *Land*, *10*(3), 231.
23. Oliveira, S., Oehler, F., San-Miguel-Ayanz, J., Camia, A., & Pereira, J. M. (2020). Modeling spatial patterns of fire occurrence in mediterranean Europe using regression and random forest. *Foresty Ecology and Management*, *275*,117 129. https://doi.org/10.1016/j.foreco.2012.03.003
24. Poudel, K. R., & Rawat, K. (2023). Comparative Analysis of Urban Area Extraction Using Different Classification Methods: A Case Study of Ghorahi Sub-Metropolitan City, Nepal. *The Himalayan Geographers*, 1-18. https://doi.org/10.3126/thg.v13i1.71342
25. Roberts, D., Mueller, N., & Mcintyre, A. (2017). High-dimensional pixel composites from earth observation time series. *IEEE Transactions on Geoscience and Remote Sensing*, *55*(11), 6254-6264. https://doi.org/10.1109/TGRS.2017.2723896
26. Shetty, S. (2019). Analysis of machine learning classifiers for LULC classification on google earth engine. University of Twente. http://essay.utwente.nl/83543/1/shetty.pdf

27. Somanathan, S. P., Kesavan, M., Parambath, S. K., Muraleedharan, B. V., Krishnan, S., & Damodharan, P. (2024). A Novel Bare Soil Index for Enhancing the Mapping of Bare Soil Area–An Indicator of Urban Expansion. *Ecological Engineering & Environmental Technology (EEET), 25*(10).
28. Sultana, S., & Inayathulla, M. (2022). Precision Land Use and Land Cover Classification Using Google Earth Engine: Integrating Random Forest and Support Vector Machine Algorithms. *Geo. Eye, 11*(2), 9-14. https://doi.org/10.53989/bu.ge.v11i2.4
29. Talukdar, S., Singha, P., Mahato, S., Pal, S., Liou, Y. A., & Rahman, A. (2020). Land-use land-cover classification by machine learning classifiers for satellite observations—A review. *Remote sensing, 12*(7), 1135. https://doi.org/10.3390/rs12071135
30. Talukdar, S., Singha, P., Mahato, S., Praveen, B., & Rahman, A. (2020b). Dynamics of ecosystem services (ESs) in response to land use land cover (LU/LC) changes in the lower Gangetic plain of India. *Ecological Indicators, 112*, 106 121. https://doi.org/10.1016/j.ecolind.2020.106121
31. Talukdar, S., Singha, P., Mahato, S., Shahfahad, Pal, S., Liou, Y.A., & Rahman, A. (2020a). Land-use land-cover classification by machine learning classifiers for satellite observations- a review. *Remote Sensing, 34* (12), 2277-2300. https://doi.org/10.3390/rs12071135
32. Tariq, A., Ali, S., Basit, I., Jamil, A., Farmonov, N., Khorrami, B., ... & Hatamleh, W. A. (2023). Terrestrial and groundwater storage characteristics and their quantification in the Chitral (Pakistan) and Kabul (Afghanistan) river basins using GRACE/GRACE-FO satellite data. *Groundwater for Sustainable Development*, *23*, 100-990. https://doi.org/10.1016/j.gsd.2023.100990
33. Thanh, Noi, P., & Kappas, M. (2018). Comparison of random forest, k-nearest neighbor, and support vector machine classifiers for land cover classification using Sentinel-2 imagery. *Sensors, 18*(1), 18. https://doi.org/10.3390/s18010018
34. Tung, D. T., Tung, N. T., Thuy, H. T., Ngoc, T. M., Huyen, D. T. T., & Linh, P. C. (2023, November). Analyzing urban expansion in Hanoi using machine learning and multi-temporal satellite imagery. In *International Conference on Geoinformatics for Spatial-Infrastructure Development in Earth & Allied Sciences* (pp. 245-263). Cham: Springer Nature Switzerland. https://doi.org/10.1007/978-3-031-71000-1_14
35. Xiong, J., Thenkabail, P. S., Tilton, J. C., Gumma, M. K., Teluguntla, P., Oliphant, A., ... & Gorelick, N. (2017). Nominal 30-m cropland extent map of continental Africa by integrating pixel-based and object-based algorithms using Sentinel-2 and Landsat-8 data on Google Earth Engine. *Remote Sensing, 9*(10), 1065. https://doi.org/10.3390/rs9101065
36. Yasin, M. Y., Abdullah, J., Noor, N. M., Yusoff, M. M., & Noor, N. M. (2022, October). Landsat observation of urban growth and land use change using NDVI and NDBI analysis. In IOP Conference Series: Earth and Environmental Science (Vol. 1067, No. 1, p. 012037). IOP Publishing.
37. Zha, Y., Gao, J., & Ni, S. (2003). Use of normalized difference built-up index in automatically mapping urban areas from TM imagery. *International journal of remote sensing, 24*(3), 583-594.

38. Zhang, C., & Li, X. (2022). Land use and land cover mapping in the era of big data. *Land, 11*(10), 1692. https://doi.org/10.3390/land11101692
39. Zhao, Z., Islam, F., Waseem, L. A., Tariq, A., Nawaz, M., Islam, I. U., ... & Hatamleh, W. A. (2024). Comparison of three machine learning algorithms using Google Earth Engine for land use land cover classification. *Rangel. Ecol. Manag. 92*, 129-137. https://doi.org/10.1016/j.rama.2023.10.007
40. Zheng, Q. H., Chen, W., Li, S. L., Yu, L., Zhang, X., Liu, L. F., ... & Liu, C. Q. (2021). Accuracy comparison and driving factor analysis of LULC changes using multi-source time-series remote sensing data in a coastal area. *Ecological Informatics*, *66*, 101457. https://doi.org/10.1016/j.ecoinf.2021.101457